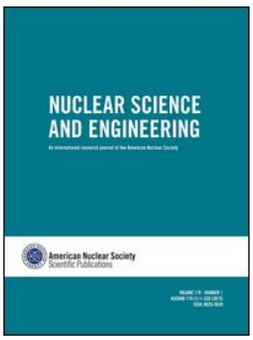

Nuclear Science and Engineering

ISSN: (Print) (Online) Journal homepage: https://www.tandfonline.com/loi/unse20

Simulation of the Melting Behavior of the UO_2-Zircaloy Fuel Cladding System by Laser Heating

L. Soldi, D. Manara, D. Bottomley, D. Robba, L. Luzzi & R. J. M. Konings

To cite this article: L. Soldi, D. Manara, D. Bottomley, D. Robba, L. Luzzi & R. J. M. Konings (2022): Simulation of the Melting Behavior of the UO_2-Zircaloy Fuel Cladding System by Laser Heating, Nuclear Science and Engineering, DOI: 10.1080/00295639.2022.2106731

To link to this article: https://doi.org/10.1080/00295639.2022.2106731

Published online: 07 Sep 2022.

NUCLEAR SCIENCE AND ENGINEERING

DOI: https://doi.org/10.1080/00295639.2022.2106731

Simulation of the Melting Behavior of the UO_2-Zircaloy Fuel Cladding System by Laser Heating

L. Soldi,[a,b] D. Manara,[a*†] D. Bottomley,[a‡] D. Robba,[a] L. Luzzi,[b] and R. J. M. Konings[a]

[a]*European Commission, Joint Research Centre, Karlsruhe, Germany*
[b]*Politecnico di Milano, Department of Energy, Nuclear Engineering Division, Via La Masa 34, 20156, Milano, Italy*

Received January 3, 2022
Accepted for Publication July 22, 2022

Abstract — *The current research focuses on laser melting and successive analysis of laboratory-scale uranium dioxide nuclear fuel samples in direct contact with Zircaloy-4 cladding. The goal was to characterize the melted and refrozen interfaces, in particular, observing local changes of the melting point and interdiffusion of fuel and cladding materials under inert gas (Ar), in the presence of hydrogen (Ar + 6% H_2) or in air. Results obtained by laser heating UO_2 pellets clad in a Zircaloy ring were interpreted in light of reference tests performed on pellets in which UO_2 and zirconium were blended in a series of given compositions. The sample composition was analyzed by scanning electron microscopy to verify the occurrence of diffusion and segregation phenomena during the laser-heating cycles. Laser-melting experiments were performed on pellets of uranium dioxide clad in Zircaloy-4 rings to simulate the configuration of a light water reactor fuel rod. Under inert gas, the material interdiffusion resulted in consistent melting point depression (of up to 200 K below the melting point of pure UO_2) at the interface between the fuel and the cladding. Experiments carried out in the presence of H_2 displayed a more limited effect on the melting temperature, but they resulted in a remarkable embrittlement of the whole structure, with large fragmentation of the Zircaloy cladding. This was probably due to the formation of brittle and highly volatile Zr hydrides. The observed melting point decrease was even more pronounced (up to over 400 K) under air in uranium-rich samples, due to the change in the stoichiometry of UO_2 in UO_{2+x}.*

Keywords — *Corium, laser heating, light water reactor, nuclear fuel, severe accidents.*

Note — *Some figures may be in color only in the electronic version.*

I. INTRODUCTION

The international community is increasingly worried about the severe consequences of global warming. The average temperature of the planet is estimated to have risen approximately 1°C from the preindustrial level.[1] The reasons behind this temperature increase are numerous and related to human activities. Among them, electricity production is one of the most impacting sources of CO_2 emissions, being mainly based on fossil fuel power plants. Nuclear energy has been acknowledged as a carbon-free source in the Intergovernmental Panel on Climate Change 1.5°C report,[1] exploiting fission chain reactions of fissile nuclides (typically ^{235}U and ^{239}Pu). However, the inclusion of nuclear and gas in the list of environmentally sustainable economic activities is still under debate in the European Union.[2] Public acceptance of nuclear energy is still an open issue, mainly because

*E-mail: dario.manara@ec.europa.eu
†Current address: European Commission, Joint Research Center, Ispra, Italy
‡Current address: Japan Atomic Energy Agency-CLADS Laboratory, Iwaki, Japan

people are concerned with the safety of nuclear power plants and the management, storage, and disposal of radioactive waste. In particular, concerns about possible catastrophic consequences of a severe accident in a nuclear power plant present a real obstacle to widespread public acceptance of nuclear energy.

Severe nuclear power plant accidents actually occurred in Three Mile Island (1979), Chernobyl (1986), and Fukushima (2011) (Ref. 3). Despite being three very different situations, their evolution and all the phenomena involved have been crucial to better understand and improve the safety of current and future reactors. The study of accident scenarios and management is now one of the most challenging topics for the civil nuclear field because of the complexity of the extreme material conditions involved and the possible events and their sequence that may occur.

Typically, a nuclear fission reactor accident is considered to be "severe" when total or partial core meltdown happens.[3–6] In these conditions, the average temperature inside the fuel pellet increases hundreds of kelvins higher than the nominal operational values. Such temperature rise may lead to local melting of the fuel, especially in the proximity of the cladding (typically made of a zirconium alloy called Zircaloy, or stainless steel). Here, lower-melting eutectics form due to the chemical interaction between fuel and cladding during normal operations and may potentially lead to liquefaction of the nuclear core. During a nuclear accident in a light water reactor (LWR), the interaction between UO_2 fuel and Zircaloy starts well below the cladding melting point (2120 K), at temperatures much lower than the actual fuel liquefaction temperature (3130 K). A U-O-Zr–rich molten material can then be formed at the UO_2-Zy interface, which may lead to partial/total dissolution of the fuel.[5,6] The composition of this liquid phase significantly depends on the accident scenario and changes with the progression of the accident.

According to diffusion-coupled results reported by Hofmann,[5] a partially liquefied material mostly containing uranium, zirconium, and oxygen may be found at the interface between UO_2 and Zircaloy already at 1773 K. Approaching the Zircaloy melting temperature, the dissolution rate significantly increases. This leads to the possible formation of a two-phase mixture comprising a UO_2-based solid fluorite phase, in which some Zr is dissolved, and a partially oxidized metallic liquid phase. Above 2500 K, the existence of a miscibility gap in the liquid phase[3–7] may contribute to corium stratification in the reactor vessel.

In this work, the melting of the fuel-cladding combination is investigated experimentally using a laser-heating approach.[7] First, pellets of Zr-UO_2 mixtures with defined compositions are studied to understand the melting temperatures of known compositions. These mixed zirconium–uranium dioxide samples were produced in an earlier international cooperation called COre LOSS during a severe accident[8] (COLOSS), in which UO_2 solubility in molten zirconium was tested. In the current work, the same material samples have been used to investigate the melting behavior of the UO_2-Zr quasi-binary system. In the second part of the current investigation, real UO_2 fuel pellets inserted in real Zircaloy-cladding rings were locally melted at the fuel-cladding interface and in the fuel bulk far from the fuel-cladding interface. Melting and freezing temperatures were observed in different positions of the combined fuel-cladding sample. The second part of the current investigation has been conducted to simulate the melting behavior of the fuel-cladding assembly in a geometry close to the one of a typical LWR fuel element. The experimental results obtained in different positions of the fuel-cladding assembly are compared to estimate the composition of the fuel-cladding mixture that may be stabilized at different spots in case of a severe nuclear accident.

The experiments were performed in inert gas (pressurized Ar at 0.3 MPa) in a hydrogen-rich reducing atmosphere (pressurized Ar + 6 mol % H_2) and also in strongly oxidizing (pressurized air) conditions. In this way, three different chemical environments were simulated, in which overheating of the fuel may occur in a nuclear power plant accident, depending on the evolution of the accident scenario. Tests under pressurized Ar were carried out as a reference case. Experiments performed under H_2-containing atmosphere simulate the conditions that can build up locally during rapid fuel and Zircaloy oxidation and water dissociation as the reactor core temperature increases in an uncontrolled fashion. The following reactions have been suggested to occur under these conditions[9,10]:

$$Zr + H_2O \rightarrow ZrO_2 + H_2 \tag{1}$$

and

$$UO_2 + xH_2O \rightarrow UO_{2+x} + xH_2 \ . \tag{2}$$

The molecular hydrogen thus produced can accumulate in the upper part of the reactor pressure vessel and in case of

vessel failure poses a high risk of explosion (concretized for example in the Fukushima Daiichi units affected in 2011).

Moreover, H_2 can react with the metallic cladding and form highly brittle and volatile Zr hydrides, which can result in rapid disaggregation or delayed cracking of the fuel-cladding system.[10] Fuel/cladding system fast heating experiments in the presence of H_2 are therefore particularly crucial for an improved understanding of the events that might occur in a LWR core meltdown accident.

Finally, some laser-heating tests carried out on a UO_2 disk in a Zircaloy ring under a strongly oxidizing atmosphere, i.e., pressurized air at 0.3 MPa, were aimed at checking how the melting behavior of the investigated UO_2-Zr mixture evolved in a laboratory-simulated case of air ingress into the melting reactor core.

The current research was partially developed as an in-kind contribution to the Organisation for Economic Co-operation and Development (OECD) Nuclear Energy Agency (NEA) project called "Thermodynamic Characterisation of Fuel Debris and Fission Products Based on Scenario Analysis of Severe Accident Progression at Fukushima-Daiichi Nuclear Power Station (TCOFF)" (Ref. 11). Thus, the current investigation was carried out in light of analysis of the severe accident progression in the Fukushima Daiichi power plant.

II. EXPERIMENTAL

II.A. Samples

The first part of the current work studied the liquid-solid transition of mixed Zr-UO_2 samples with given compositions in the full composition range. The samples analyzed here were fabricated by powder metallurgy and high-temperature sintering under inert atmosphere in the COLOSS project[8] in order to produce reference data and better understand the solubility of nuclear fuel in molten zirconium. Please note that hereinafter, the resulting mixtures will be called COLOSS samples. Seven compositions of COLOSS samples were tested. The sample compositions were cross-checked by scanning electron microscopy (SEM) and energy-dispersive X-ray (EDX) analysis (SEM-EDX) and corresponded to the nominal one within the method uncertainty. They are reported together with their melting temperatures in Table I in Sec. III. Data obtained in this part of the work were then compared with the results obtained in melting experiments performed at the fuel-cladding interface.

To this purpose, the second part of the current investigation was focused on the behavior of commercial UO_2 fuel pellets inserted in a Zircaloy-4 ring (Fig. 1). The aim of this kind of setup was to reproduce the geometry of a real fuel rod at the scale of a single pellet. This geometry was interesting to understand how fuel and cladding could interact in the first stages of a loss-of-coolant accident. Observing the melting temperature evolution of this mixture helped to estimate the composition of corium at this stage.

II.B. Postmelting SEM-EDX Characterization

Postmelting sample analysis was locally performed by means of SEM-EDX in order to estimate the elemental composition of the formed phases. These analyses were carried out with a Philips XL 40 scanning electron microscope, equipped with tungsten filament and a secondary electron (SE) and backscattered electron (BSE) detector or a Vega-Tescan scanning electron microscope equipped with an Oxford EDX and wavelength dispersive X-ray spectrometry system. Samples were mounted on metallic sample holders fixed by screws or with carbon tape (the conductivity of which helped avoid specimen charging). Both SE and BSE modes were employed to produce the SEM images. Particularly, the latter permits the distinction between darker areas or phases richer in lighter elements, in this case Zr-rich (Z_{Zr} = 40), and brighter regions richer in heavy elements, such as U (Z_U = 92) areas. In addition, EDX measurements were used to specify the compositions of the materials at various spots (~1- to 3-μm-diameter point analyses), with a relative accuracy of ±2.5%.

II.C. The Laser-Heating Method

The current research has been carried out at the European Commission's Joint Research Center (JRC) of Karlsruhe (Germany), where a laser-heating facility is employed for the investigation of the high-temperature behavior of refractory radioactive materials (Fig. 2). The current setup is described in detail in Refs. 12 and 13. Here, the main instruments and the method are summarized without focusing on the calibration and the mathematical formulation. The setup essentially consists of an autoclave, one laser, two different pyrometers, and an infrared thermal camera.

Laser-heating experiments were carried out in a cylindrical vessel (autoclave). A sapphire window (optical transmittance = 0.86 in the visible and near-infrared range) allowed the laser to reach and heat the sample

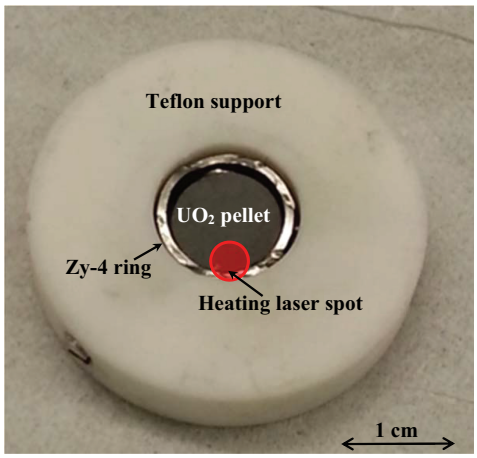

Fig. 1. A UO_2 fuel pellet inserted in Zircaloy-4 rings in order to reproduce on a single-pellet size the geometry of a real LWR fuel element.

inside. Thanks to a pump system, up to 0.3 MPa of overpressure of a selected gas or gas mixture can be set inside the autoclave.

This overpressure limits possible evaporation of volatile species during the heating and imposes chemical conditions to the closed environment inside the vessel. The sample had the shape of a disk placed in the autoclave with the help of graphite screws. It was heated by laser shots emitted by a TRUMPF Nd: YAG source at 1064.5 nm. Despite being a continuous-wave laser, 1-ms pulses can be generated with the help of a chopper. The laser was focused on the circular surface of the sample. In the first part of the investigation, performed on COLOSS samples, the heating laser was focused on a round spot (5 mm in diameter) near the center of the pellet's flat face. The sample was initially heated for a few seconds by the laser beam at low power in order to stabilize the material at higher temperature (around 1500 K) and reduce the thermal stresses occurring with very high heating rates (on the order of thousands of kelvins per second).

Two pyrometers were used to measure the evolution of the temperature of the sample surface, given its emissivity: a fast pyrometer at 655 nm, calibrated against a standard W lamp; and a multichannel spectropyrometer, collecting radiance spectra at 256 wavelengths from 488 to 1011 nm, which was calibrated against a blackbody source up to 3000 K (Refs. 12 and 13). The latter spectropyrometer permitted the simultaneous determination of the sample temperature and normal spectral emissivity (NSE) $\varepsilon\lambda$, which is needed to convert radiance into temperature.[14,15] Here, the NSE of nuclear fuel samples interacting with Zircaloy cladding has been obtained in the hypothesis that the emissivity is wavelength independent both for UO_2 and Zircaloy in the spectral range of the current spectrometer, as reported in previous research[16,17]. It is hard to tell whether this hypothesis is still valid for the liquid mixture. This certainly constitutes an additional source of uncertainty for the measured temperature when the material is molten. However, no obvious discontinuity was observed in the reported thermograms, which might be associated with a sharp change in the emissivity behavior upon the solid-phase–liquid-phase transition. Moreover, such an additional uncertainty source is not so relevant for the current solidification point data, which were measured on the already resolidified surface.

Once the preheating was performed and the material was stabilized at high temperature, a high-power short-duration pulse was sent to the sample surface, causing a sudden increase of the temperature, leading to its melting. The temperature-time curve of the laser-heated specimen as a function of time during the high-power laser pulse, commonly referred to as a thermogram, was used to perform thermal analysis.

By heating the sample only locally, the melted material was not in contact with any other element, except the sample material itself. In this approach, the liquid material is self-contained, which minimized any external chemical contamination.

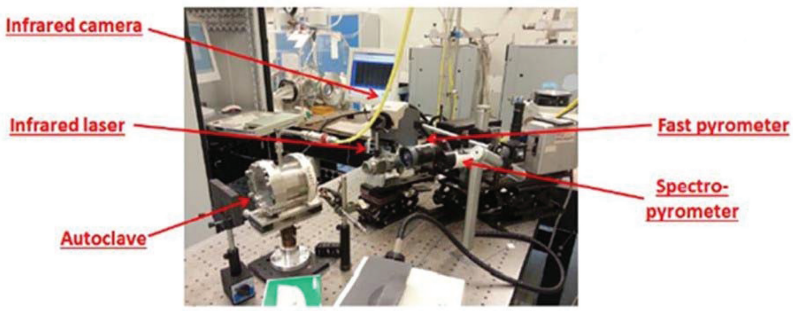

Fig. 2. Laser-heating facility at JRC Karlsruhe.

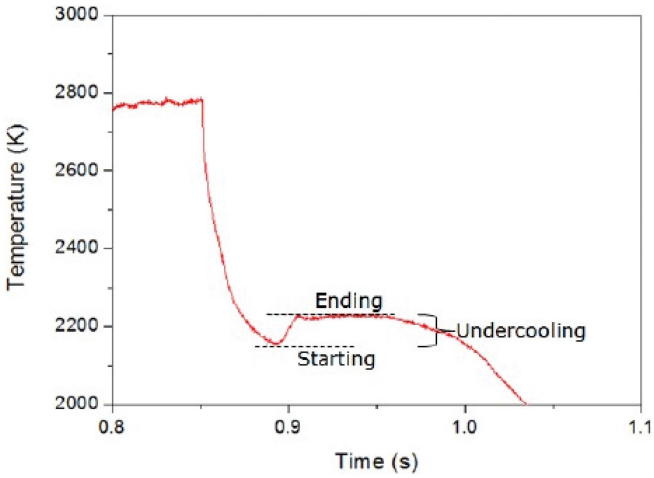

Fig. 3. Example of a thermogram of the UO_2-Zr system, where the start and the end of the solidification, as well as the undercooling, are highlighted. Source: OECD (2021) (Ref. 11).

Inflections or thermal arrests in the thermograms give information related to phase transitions (e.g., solidus, liquidus, and isothermal phase transformations). Note, however, that during the laser pulse part of the experiments, the intense laser irradiation (some kW/cm^2) induced a quick temperature increase in the material (some 1000 K/s), which made it hard to detect phase transitions on the heating flank of the thermograms. Inflections and thermal arrests were more easily detected during natural cooling of the liquid sample surface back to the solid state and to room temperature.

The current analysis was therefore performed on the cooling flank of the thermograms only. After the end of the laser pulse, the sample temperature dropped quickly through the solidification temperature range. During the phase transition a clear thermal arrest was observed, according to the Gibbs phase rule, as the solidification enthalpy was released by the freezing material. The time extent of such thermal arrest depended on the amount of freezing material and the solidification enthalpy.

Solidification took some time, on the order of 100 ms, starting from the liquid-solid interface and moving to the central part of the melt. In this time interval, the temperature of the central part of the liquid on which the pyrometer was focused regularly decreased below the solidus, meeting the so-called liquid undercooling conditions.

Under these conditions, the temperature detected by the pyrometer was lower than the solidification point, even if a pure—undercooled—liquid phase was still present. When this metastable liquid started to freeze, solidification enthalpy was released, and the material temperature increased again, as shown in Fig. 3. The solidification arrest thus immediately followed the undercooling stage. The most significant uncertainty sources related to the laser heating and multichannel pyrometry have been combined, according to the independent error propagation law,[12] and expanded to yield relative temperature uncertainty bands corresponding to 2 standard deviations (k = 2 coverage factor). These uncertainty contributions stem from the uncertainty in the pyrometer calibration δT, the NSE assessment $\delta T\varepsilon\lambda$, and the experimental data scatter on the current phase transition radiance temperature data $\delta T\lambda m$, the latter being the main source of uncertainty:

$$\delta T_m = \sqrt{\delta T^2 + \delta T_{\varepsilon\lambda}^2 + \delta T_{\lambda m}^2} \quad . \tag{3}$$

The resulting uncertainty is about 30 K at 3000 K with calculated uncertainty values reported for each measurement.

III. RESULTS AND DISCUSSION

III.A. COLOSS Samples

COLOSS samples with seven different compositions were laser melted. Their nominal compositions and melting temperatures are reported in Table I. Their compositions were cross-checked by SEM-EDX and corresponded to the nominal ones within the characterization method uncertainty (±2.5 mol %), on a spot corresponding to the laser-heated area. These samples consisted of separated phases at room temperature. However, the phases got mixed into a single liquid when laser heated beyond the melting temperature. Therefore, with the current approach it was possible to investigate how the various UO_2 + Zr mixtures of the COLOSS sample solidified when they were cooled from a single-phased liquid. Four heating laser shots were successively applied to each sample. The reported temperatures are the average of the four measurements performed on each sample, with the corresponding standard deviation over the four shots.

The tests were performed first in inert conditions (autoclave filled with Ar) and then in a reducing environment (a mixture of Ar + 6 mol % H_2). The different chemical environments led to variations in the measured melting temperatures for each given composition, up to approximately 200 K in the composition range between 20 mol % UO_2 and 40 mol % UO_2. A major role of hydrogen was also observed. In fact, all the samples

TABLE I

Compositions and Results of COLOSS Samples*

Name	UO_2 (mol %)	Zirconium (mol %)	Pyrometer Temperature (/K)		Spectropyrometer Temperature (/K)	
			Inert	Reducing	Inert	Reducing
COLOSS-10	10	90	2305 ± 13	2354 ± 16	2316 ± 15	2360 ± 16
COLOSS-20	20	80	2230 ± 31	2394 ± 20	2212 ± 12	2240 ± 16
COLOSS-40	40	60	2390 ± 9	2592 ± 11	2418 ± 24	2503 ± 18
COLOSS-60	60	40	2641 ± 8	2660 ± 19	2620 ± 21	2606 ± 21
COLOSS-80	80	20	2781 ± 19	2809 ± 14	2756 ± 24	2890 ± 20
COLOSS-90	90	10	3066 ± 54	2982 ± 80	3180 ± 29	2950 ± 62
COLOSS-95	95	5	3065 ± 42	3147 ± 21	3156 ± 20	3162 ± 41

*Source: OECD (2021) (Ref. 11).

melted in the presence of hydrogen became more brittle and presented several cracks on the surface.

The melting temperatures of the available COLOSS samples strongly evolved depending on the composition. CALPHAD thermodynamic calculations performed by Quaini et al.[7] for the Zr-UO_2 system are compared with the experimental measurements for both inert and reducing conditions (Figs. 4 and 5, respectively). As already pointed out in Sec. II, the results presented here are directly compared to the liquidus evolution. The experimental melting temperatures for COLOSS-60 and COLOSS-80 fall in the liquid miscibility gap domain[7] (between approximately 50 mol % UO_2 and 85 mol % UO_2), where two immiscible liquids are at equilibrium. The current approach

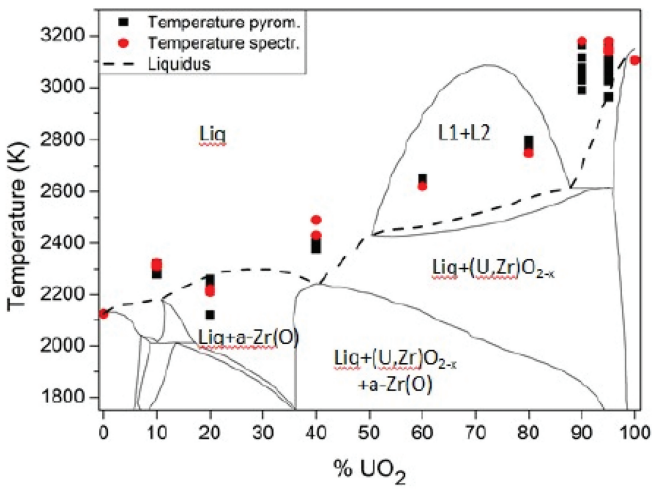

Fig. 4. Comparison between the computed thermodynamic model of the Zr-UO_2 system proposed by Quaini et al.[7] and the melting temperature of the COLOSS samples in inert atmosphere (Ar). Temperature and composition uncertainty bands reported in Table I are not plotted here. Source: OECD (2021) (Ref. 11).

was not suited to detect the two-liquid formation because the latent heat associated with such transition is not high enough to result in any detectable thermal arrest in the measured thermogram.

The model for the Zr-U-O system is based on a limited set of experimental data, so it is difficult to state whether the thermodynamic model well represents the real behavior of the system. Certainly, the experimental measurements are performed in different chemical conditions, so it is possible that the global composition of the samples during the laser tests moved away from the Zr-UO_2 section. This may also partially explain the disagreement between the experimental results and the CALPHAD estimation. Still, the experimental data are in good qualitative agreement with the computed melting temperatures of the Zr-UO_2 section.

Postmelting sample analysis was locally performed by means of SEM-EDX. In the as-fabricated samples, UO_2 and Zr are heterogeneously distributed, and the local amount of one or the other component is quite different from the nominal one. However, the melted volume is large enough to be unaffected by the local distribution of the two constituents and be representative of the nominal composition of the sample itself, assuming that the two components are homogeneously mixed when the laser heats the sample very quickly into the liquid phase.

Examining the samples after the laser-heating treatment, at least three areas can be identified (Fig. 6 and compositions in Table II): in the central part of the melted zone, where UO_2 and Zr are homogeneously distributed; in a transition zone, in which small portions of two distinct phases are segregated; and finally, in the unmolten part of the sample, with the same characteristics as described before for the as-fabricated material.

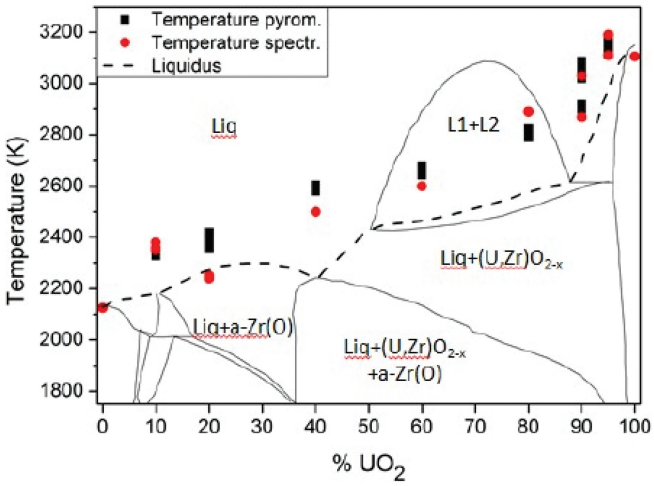

Fig. 5. Comparison between the computed thermodynamic model of the Zr-UO_2 system proposed by Quaini et al.[7] and the melting temperature of the COLOSS samples in reducing atmosphere (Ar + 6% H_2). Temperature and composition uncertainty bands reported in Table I are not plotted here. Source: OECD (2021) (Ref. 11).

TABLE II

Compositions of Phases Referred to Fig. 5 from EDX Analysis (Excluding O)*

Point Number	Uranium (mol %)	Zirconium (mol %)
1	4.4	95.6
2	36.8	63.2
3	2.9	97.1
4	52.9	47.1
5	2.2	97.8

*Each Measurement is an average of four points of the same phase. Source: OECD (2021) (Ref. 11).

The morphology of the quenched phases is qualitatively linked to the temperature distribution induced in the sample surface by the laser pulses. The center of the spot reached the highest temperature during the experiment, and therefore, the quenched solidified material was representative of the high-temperature liquid, in which the components are well mixed. The composition observed in this part of the sample was thus close to the nominal one. However, no assumption could be made on the phases present in this resolidified region. Farther away from the center, the

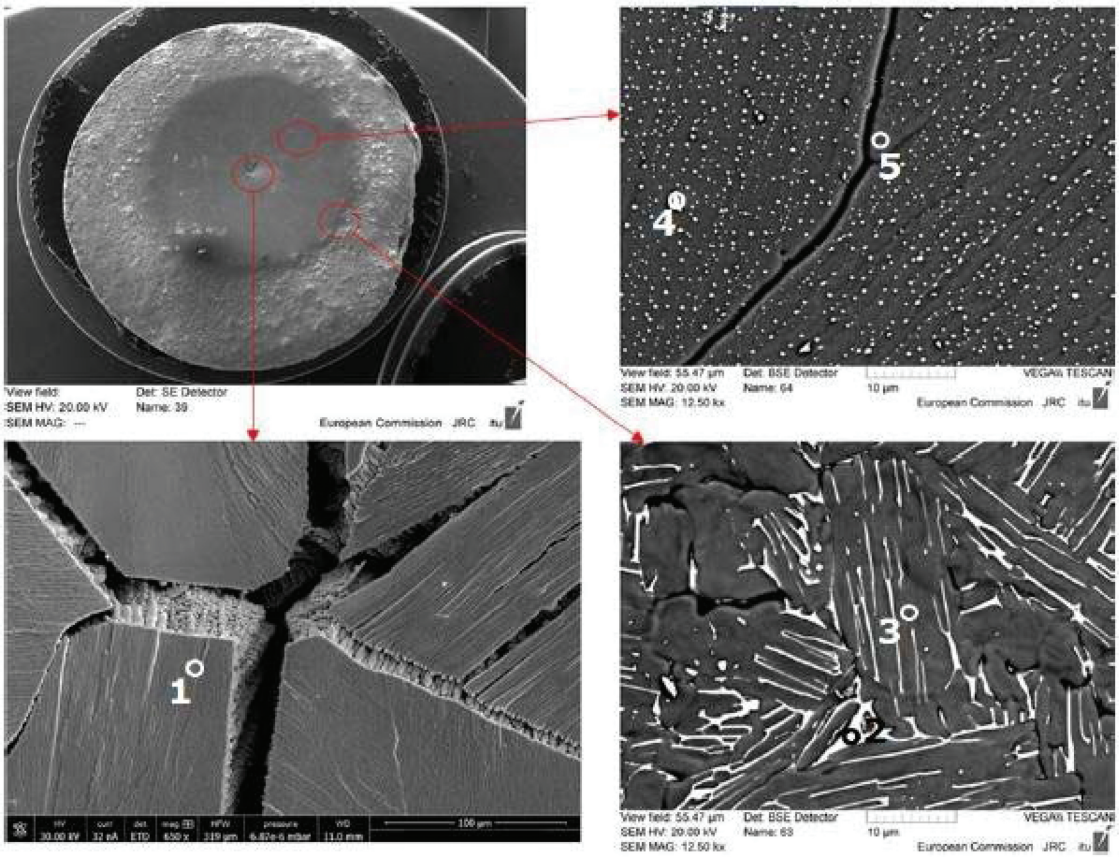

Fig. 6. SEM images of COLOSS-10 in three regions of the melted area. The compositions of the indicated phases are reported in Table II. Source: OECD (2021) (Ref. 11).

maximum temperature reached during laser irradiation decreased more and more until a two-phase zone was produced during the heating stage. Here, depending on the composition of the sample, the constituent in the smaller fraction started to grow forming tiny spots in the matrix of the major constituent, following the boundaries of the two-phase regions of the phase diagrams reported in Figs. 4 and 5.

In the BSE images on the right side of Fig. 6, it is obvious that a bright phase richer in uranium was formed upon solidification as little droplets embodied in a Zr matrix. However, according to the phase diagram reported in Figs. 4 and 5, for the COLOSS-10 sample, UO_2 is not supposed to form since the global composition of the sample is far from the uranium oxide side of the quasi-binary diagram. It is most likely that the U initially solubilized in the alpha-Zr phase at high temperature was rejected due to a drastic drop of the solubility during cooling. These tiny spots became bigger and bigger in the periphery of the interaction zone, in agreement with a reduced solubility in the areas with a lower temperature. This may be also due to the change in the composition and the occurrence of a peritectic transition around 2000 K between 8 mol % of UO_2 and 20 mol % of UO_2 in the phase diagram of Figs. 4 and 5. The microstructure seems to suggest that a peritectic or a eutectic transition took place during cooling. Finally, the temperature profile in the farthest part of the sample was not high enough to promote a phase transition, so the initial composition and morphology of the sample were maintained.

In samples with intermediate compositions, a ring richer in Zr was found in the periphery of the laser-irradiated area (Fig. 7). In samples with UO_2 molar fractions larger than 20 mol %, the phase equilibria reported in Figs. 3 and 4 are in line with a possible segregation of high-melting U-rich material in the central part and lower melting species richer in Zr in the outer ring of the laser-irradiated area. The periphery area was in fact characterized by a much lower temperature reached during the laser-heating stage, so the Zr solidifying at lower temperature[16,17] started forming columnar grains from the outside, growing toward the center. The remaining liquid uranium-rich phase in the center of the laser-heated pellet surface tended to flow toward the Zr ring because of the higher melting temperature.[11]

III.B. UO_2 + Cladding

The second part of this investigation was focused on a situation where a UO_2 pellet was inserted in a Zircaloy-4 ring. The aim of this kind of setup was to reproduce the geometry of a fuel rod. In the case of a severe accident, the situation in the early stages cannot be represented by a COLOSS sample, where UO_2 and Zr are mixed together from the beginning. Instead, the first element to heat up is the fuel and, a few instants later, the external cladding. This geometry is interesting to understand how fuel and cladding interact in the first stages of a loss-of-coolant accident. Observing the melting temperature evolution of this mixture can help estimate the composition of corium at this stage. Such data are fundamental for simulating the behavior of corium with a dedicated code and then predicting the possible evolution of the accident.

This type of experiment was performed by pointing the laser beam at the periphery of the fuel pellet, in contact with the Zircaloy ring, as shown in Fig. 1, to simulate the accident scenario. Once the sample was placed in the autoclave and the Ar atmosphere was stabilized at 0.3 MPa, the sample was subjected to multiple laser pulses. Both the monochromatic pyrometer and the multichannel

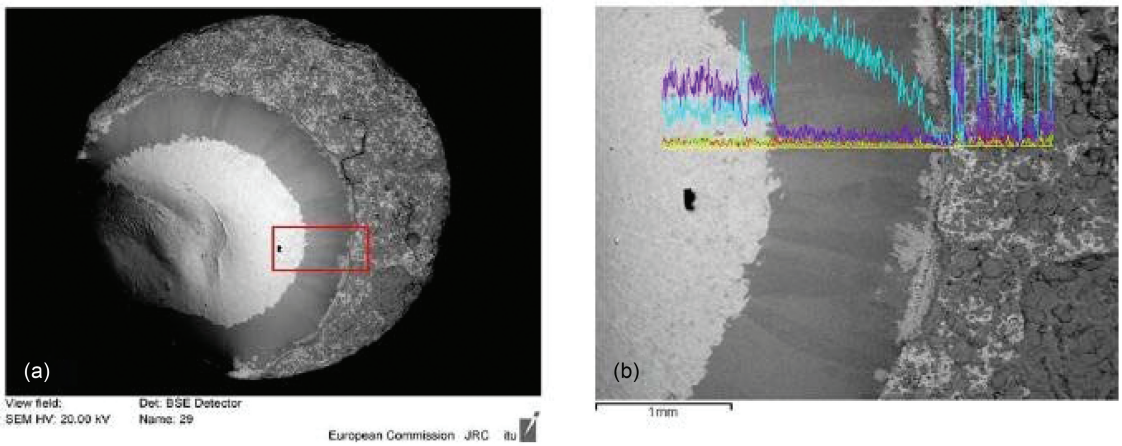

Fig. 7. (a) SEM image of COLOSS-20, where a dark Zr ring appears around the melted area and (b) zoom in the periphery of the melted area, with the evolution of Zr (light blue) and U (violet) composition along the line. Source: OECD (2021) (Ref. 11).

spectropyrometer were focused on the heated area: The first one was used to observe the evolution of the temperature at the center of the laser spot while the second measured the temperature in the contact area between the pellet and the Zircaloy ring. The melting/freezing thermal arrest temperature difference between the two instruments was significant. It amounted to more than 100 K during the same pulse pointing in very close areas, as shown in Fig. 8. The observed difference indicates that zirconium/uranium dioxide interdiffusion took place even with one single laser pulse heating at high temperature.

Even after a first laser pulse, visual inspection of the sample revealed obvious melting and a partial interaction between the fuel and the cladding. When several laser shots were repeated under pressurized argon on the same area measuring each thermal arrest, the transition temperature detected in the UO_2 bulk decreased by about 200 K along the series of pulses, from 3120 K recorded during the 1st shot, which is the melting temperature of pure uranium dioxide, to about 2950 K at the 14th pulse, repeatable through to the 16th pulse (Figs. 9 and 10). After each shot, the quantity of melted material increased, and the corresponding melting/solidification temperature decreased, approximately following the phase boundaries of Figs. 4 and 5. When the measured solidification temperature was stabilized on a repeatable value, such value was assumed to correspond to the melting point of an equilibrium composition, reached through vaporization and diffusion in the liquid.

Fuel and cladding mixed together in the melt, progressively changing the composition and, consequently, the material properties. After each shot, the temperature decreased at every laser pulse until a constant value was reached, corresponding to the equilibrium composition. In fact, no further melting temperature drop lower than 2900 K was observed

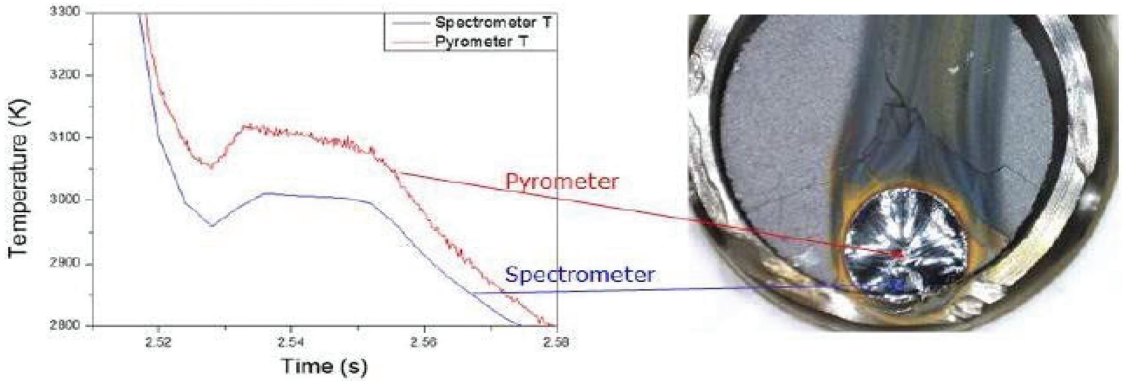

Fig. 8. Comparison between the thermograms obtained by two different pyrometers, one monochromatic and one multichannel (here referred to as Pyrometer and Spectrometer, respectively), during the melting of a UO_2 fuel sample mounted inside a real Zircaloy-cladding ring. Source: OECD (2021) (Ref. 11).

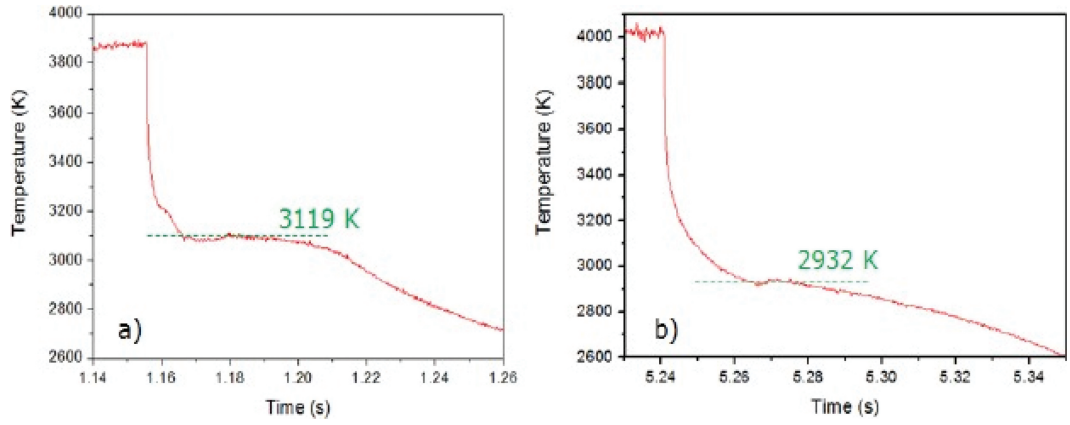

Fig. 9. Comparison between the thermograms obtained by the monochromatic pyrometer focused in the middle of the melted spot of a UO_2 fuel sample mounted inside a Zircaloy-cladding ring in inert atmosphere after (a) the 1st laser pulse and (b) after the 16th laser pulse. Source: OECD (2021) (Ref. 11).

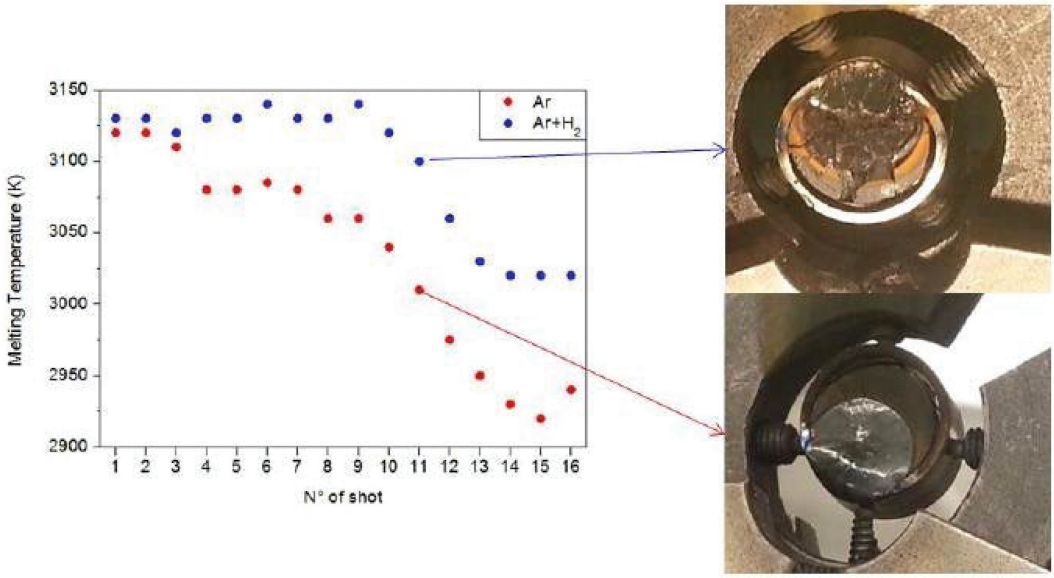

Fig. 10. Evolution of the observed melting temperature after each laser pulse, in inert (pressurized Ar) and reducing (pressurized Ar + H_2) conditions. The pictures on the right show the samples after the melting/freezing experiments in the two cases. Temperature uncertainty bands are not plotted here. Source: OECD (2021) (Ref. 11).

after 14 pulses (Fig. 10). From a nuclear safety point of view, this decrease in the melting temperature of the fuel is of some importance and should be taken into account in the safety systems design.

The final, stabilized melting/freezing temperature of these samples laser heated inside a Zircaloy cladding are compared with the results of the COLOSS samples shown above. From this comparison, one can estimate that the amount of Zr that has mixed with the fuel during the laser-heating experiments carried out under pure pressurized Ar was between 10 mol % and 20 mol %. Also, in this case, laser-melted and refrozen samples were analyzed by means of SEM-EDX to investigate the amount of Zr present in the fuel. In fact, it is possible to observe that about 17 mol % of Zr mixed with the UO_2 matrix, even at hundreds of micrometers away from the interface with the cladding ring (Fig. 11 and compositions reported in Table III). As previously noted with the COLOSS samples, a plume rich in Zr is often found around the laser-heated area. It is also worth mentioning that in the melted and refrozen fuel area, some islands richer in Zr can be found. This type of local and fragmented Zr segregation was not observed in the COLOSS samples. Thus, this different morphology of Zr-segregated phases may be due to the different starting conditions. In fact, in the case of COLOSS, UO_2 and Zr were mixed together from the beginning, and Zr segregation can happen because the phases solidify at different temperatures. In the case of a UO_2 pellet laser heated inside a Zircaloy-cladding ring, the two constituents were physically separated at the beginning, and therefore, part of the Zr did not completely interact with UO_2.

Diffusion could occur from the Zircaloy cladding into the molten fuel, resulting in the formation, upon inhomogeneous freezing, of segregated phases richer in Zr. Moreover, depending on the initial orientation of the heating laser spot with respect to the fuel + cladding ring assembly, a vapor plume originating from molten zirconium could be mixed with the freezing UO_2 above it, resulting in a dispersion of Zr-rich microparticles in the resolidified phase. These particles richer in Zr have dimensions of few tens of micrometers. Such heterogeneous distribution of Zr is much more evident in the proximity of the Zircaloy ring and contributes significantly to the melting temperature drop.

Up to this point, the results refer to samples melted in an inert condition, using Ar as filling gas in the autoclave. Some more experiments using realistic geometry were performed in reducing (using a mixture of Ar and H_2) and oxidizing (with pressurized air) environments.

The observed material behavior was different if the same laser-heating tests were repeated in Ar + 6 mol % H_2. The different evolution of experiments performed under Ar or under Ar + H_2 is shown in the left part of Fig. 10. Under Ar + H_2, only a little drop in the phase transition temperature over successive shots was observed, and even after several shots, the melting point decrease was around 100 K, i.e., about one-half

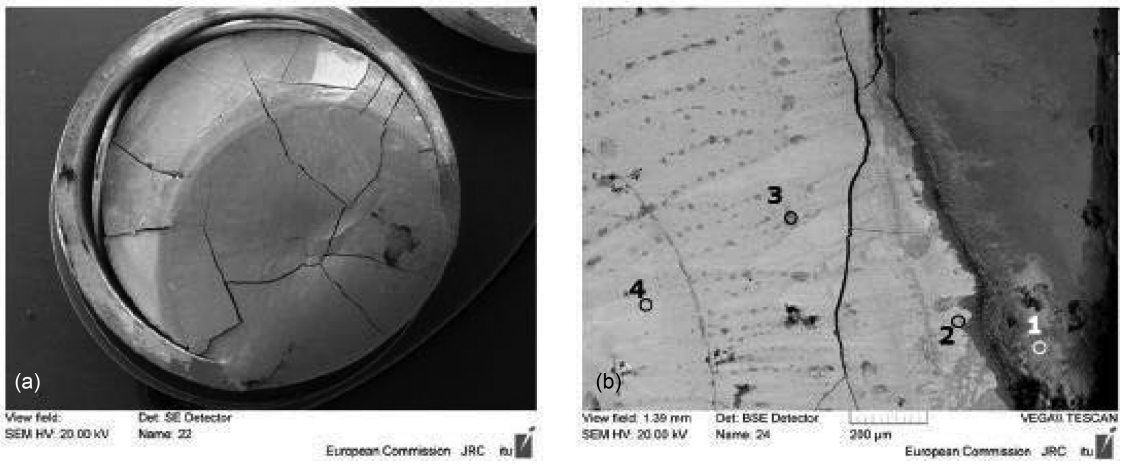

Fig. 11. SEM images of (a) the posttreatment sample in realistic geometry and (b) zoom in the periphery area. The composition of the selected point is reported in Table III. Source: OECD (2021) (Ref. 11).

TABLE III

Compositions of Phases Referred to by EDX Analysis (Excluding O)*

Point Number	Uranium (mol %)	Zirconium (mol %)
1	14.6	85.4
2	79.2	20.8
3	13.1	86.9
4	82.1	17.9

*Source: OECD (2021) (Ref. 11).

of the one recorded under inert atmosphere. A tentative explanation of this effect is that hydrogen may react with Zircaloy and form Zr-based hydrides when the temperature is still low. Such hydrides are highly volatile, and their presence could not be detected in the postmelting material characterization. However, they could in fact hinder Zr diffusion into the UO_2 matrix during heating, just because of their high volatility. The lower diffusion of Zr in the UO_2 melt resulted in a smaller or irrelevant decrease of the phase transition temperatures. From the mechanical point of view, similarly to what was observed in the COLOSS reference samples, the presence of hydrogen caused a remarkable embrittlement of the whole structure. In the presence of hydrogen, the Zircaloy ring was cracked or even fragmented after the laser-heating cycles (top-right image in Fig. 10).

Such a deterioration of the sample morphology may have been responsible for the observed melting/freezing point depression, more than the very limited Zr diffusion. The current observations confirm that in the case of a nuclear loss-of-coolant accident, significant degradation of fuel-cladding assembly mechanical stability can occur because of high-temperature interaction with a hydrogen-containing atmosphere. It is also possible that the observed embrittlement was linked to the formation of Zr-based hydrides. Unfortunately, no evidence of hydride formation was found in the SEM images or EDX spectra, certainly due to the high volatility and reactivity of such hydrides.[10]

Comparing these latter solidification temperature data recorded under $Ar + H_2$ with the solid/liquid transition lines computed by CALPHAD (Fig. 5), one can estimate in this case a lower diffusion of Zr into UO_2, indicatively lower than 10 mol %. In this case, the EDX analysis could not help in determining a more precise amount of diffused Zr because of the unavoidable reaction with the ambient air when the UO_2 fuel pellet + Zircaloy ring was removed from the laser-heating autoclave.

A few extra tests were also performed in the oxidizing condition, filling the autoclave with pressurized air at 0.3 MPa. The main goal of these tests was to check how the melting behavior of the investigated UO_2-Zr mixture evolved in the case of air ingress.

Figure 12 shows two thermograms recorded at the interface between a UO_2 pellet and a Zircaloy ring during the first and the fifth laser pulses, respectively, of a series of eight melting/freezing cycles in pressurized air. Under these conditions, the melting temperature drop is much more pronounced than in the two cases above. The solid/liquid transition occurs at lower and lower temperatures over the successive laser pulses. The solidus arrest stabilizes around 2500 K. This temperature is significantly lower than the solidus/liquidus temperatures assessed by Quaini et al.[7] for the UO_2-ZrO_2

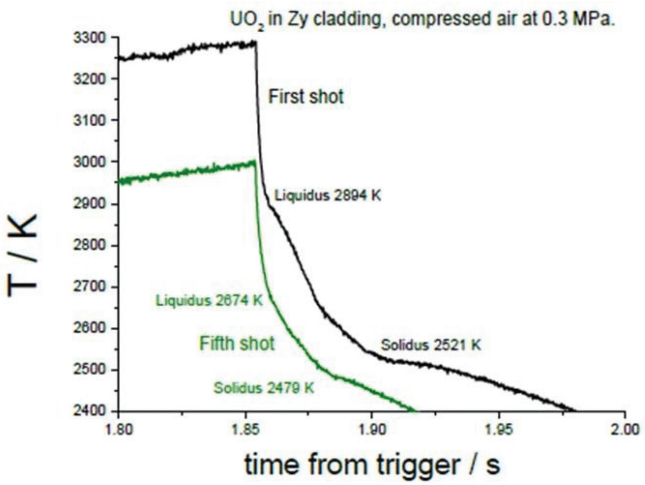

Fig. 12. Thermograms of the first and fifth pulses in a series of eight laser thermal cycles performed on UO_2 fuel sample mounted inside a real Zircaloy-cladding ring under compressed air at 0.3 MPa. Source: OECD (2021) (Ref. 11).

system. Therefore, it can certainly be ascribed to the formation of higher uranium oxides possibly also containing Zr traces.[18] In fact, the presence of oxygen surely changes the chemical behavior of U, promoting the change in the stoichiometry of the uranium dioxide from UO_2 in UO_{2+x}, characterized by lower melting temperature. The current results indicate that air ingress inside a damaged reactor pressurized vessel can dramatically change both the thermal and the chemical equilibria defining in-vessel corium composition and its properties. The current data can therefore bring some important additional input to existing approaches to in-vessel corium analysis and management (see, for example, Refs. 3, 19, 20, and 21).

IV. CONCLUSIONS

The laser-heating experiments performed in the current research on UO_2-Zr reference samples and on UO_2-Zircaloy assemblies under different atmospheres permitted observation of the following effects:

1. The solid/liquid boundary qualitatively follows the shape of the liquidus recently reported in CALPHAD optimization of the UO_2-Zr quasi-binary system, although the current experimental solid/liquid thermal arrest points mostly lie at higher temperature than the calculated boundary.

2. Diffusion of Zr into UO_2 reduces the fuel melting/freezing temperature, in agreement with the CALPHAD-optimized phase diagram, when UO_2 fuel and Zircaloy cladding are laser melted together; after 14 to 16 laser pulses, the observed melting/freezing temperature stabilizes around 2930 K for samples heated in Ar and around 3025 K for samples heated in Ar + 6% H_2.

3. Combining SEM/EDX analyses with the laser-melting experiments, one can estimate that the diffusion of Zr into the UO_2 fuel matrix leads to a stable Zr content between 15 mol % and 20 mol %. Such content is close to zero in samples laser heated in the presence of hydrogen, most probably due to the formation of brittle and volatile zirconium hydrides.

4. The presence of hydrogen in the laser-heating autoclave caused an embrittlement of the sample during the laser pulses, most probably due to the formation of hydrides. In these cases, samples were cracked or even fragmented at the end of the thermal cycles. Moreover, quick oxidation of these samples was unavoidable when they were put in contact with air. The current observations also indicate that in the case of a nuclear loss-of-coolant accident, significant degradation of the fuel-cladding assembly mechanical stability can occur as a result of the high- temperature interaction with a hydrogen-containing atmosphere.

5. The observed melting/freezing temperatures decreased well below 2700 K much more rapidly if UO_2 fuel and Zircaloy cladding were laser melted together in pressurized air. This is certainly due to the prompt formation of lower melting, uranium oxides with O/U > 2, i.e., UO_{2+x}.

The current research highlights the importance of the chemical environment effects on the processes leading to in-vessel corium formation, on the nature of corium itself, and on its melting/freezing behavior. The information conveyed by the reported results will be useful for improved in-vessel corium formation models in severe accident codes that are used for corium prediction and management. In the particular context of the current research, this information will also be useful for a deeper understanding of the accident progression in the Fukushima Daiichi power plant.

Acknowledgments

L. S. acknowledges the EURATOM FP7 project GENTLE (contract number 323304) for supporting his stay at JRC Karlsruhe. The work in the current publication was part of an in-kind contribution by JRC Karlsruhe to the OECD NEA TCOFF project; www.oecd-nea.org/science/tcoff/.

Disclosure Statement

No potential conflict of interest was reported by the author(s).

Data Availability Statement

Raw data were generated at JRC Karlsruhe. Derived data supporting the findings of this study are available from the corresponding author (D. M.) on reasonable request.

ORCID

D. Manara http://orcid.org/0000-0002-0767-9859

References

1. "Global Warming of 1.5°C. An IPCC Special Report on the Impacts of Global Response to the Threat of Climate Change, Sustainable Development, and Efforts to Eradicate Poverty," V. MASSON-DELMOTTE et al., Eds., Intergovernmental Panel on Climate Change (2018).
2. "Taxonomy: MEPs Object to Commission's Plan to Include Gas and Nuclear Activities"; https://www.europarl.europa.eu/news/en/press-room/20220613IPR32812/taxonomy-meps-object-to-commission-s-plan-to-include-gas-and-nuclear-activities (current as of Jan. 3, 2022).
3. *Nuclear Power Reactor Core Melt Accidents: Current State of Knowledge*, D. JACQUEMAIN et al., Eds., Institut de Radioprotection et de Sûreté Nucléaire (2015); https://www.irsn.fr/EN/Research/publications-documentation/Scientific-books/ (current as of Jan. 3, 2022).
4. R. R. HOBBINS et al., "Molten Material Behavior in the Three Mile Island Unit 2 Accident," *Nucl. Technol.*, **87**, 1005 (1989); https://doi.org/10.13182/NT89-A27692.
5. P. HOFMANN, "Current Knowledge on Core Degradation Phenomena, A Review," *J. Nucl. Mater.*, **270**, 194 (1999); https://doi.org/10.1016/S0022-3115(98)00899-X.
6. P. HOFMANN and C. POLITIS, "The Kinetics of the Uranium Dioxide—Zircaloy Reactions at High Temperatures," *J. Nucl. Mater*, **87**, 375 (1979); https://doi.org/10.1016/0022-3115(79)90575-0.
7. A. QUAINI et al., "Contribution to the Thermodynamic Description of the Corium—The U-Zr-O System," *J. Nucl. Mater.*, **501**, 104 (2018); https://doi.org/10.1016/j.jnucmat.2018.01.023.
8. B. ADROGUER et al., "Core Loss During a Severe Accident (COLOSS)," *Nucl. Eng. Des.*, **235**, 173 (2005); https://doi.org/10.1016/j.nucengdes.2004.08.050.
9. J. O. HENRI, "The Effects of Hydrogen Generation on Radioactive Waste Handling Technology," *Nucl. Technol.*, **87**, 729 (1989); https://doi.org/10.13182/NT89-A27665.
10. D. O. NORTHWOOD and U. KOSASIH, "Hydrides and Delayed Hydrogen Cracking in Zirconium and Its Alloys," *Int. Metals Rev.*, **28**, 92 (1983); https://doi.org/10.1179/imtr.1983.28.1.92.
11. "Thermodynamic Characterisation of Fuel Debris and Fission Products Based on Scenario Analysis of Severe Accident Progression at Fukushima-Daiichi Nuclear Power Station (TCOFF)," Organisation for Economic Co-operation and Development, Nuclear Energy Agency (2021); https://www.oecd-nea.org/science/tcoff/ (current as of Jan. 3, 2022).
12. D. MANARA et al., "New Techniques for High-Temperature Melting Measurements in Volatile Refractory Materials via Laser Surface Heating," *Rev. Sci. Instrum.*, **79**, 113901 (2008); https://doi.org/10.1063/1.3005994.
13. D. MANARA et al., "Laser-Heating and Radiance Spectrometry for the Study of Nuclear Materials in Conditions Simulating a Nuclear Power Plant Accident," *J. Vis. Exp.*, **130**, e54807 (2017); https://doi.org/10.3791/54807.
14. D. P. DEWITT and G. D. NUTTER, *Theory and Practice of Radiation Thermometry*, John Wiley & Sons (1988).
15. G. NEUER et al., "Critical Analysis of the Different Methods of Multiwavelength Pyrometry," *Temperature: Its Measurement and Control in Science and Industry*, Vol. 6, No. 1, p. 787, J. F. SCHOOLEY, Eds., American Institute of Physics, New York (1992).
16. A. QUAINI et al., "Laser Heating Investigation of the High-Temperature Interaction Between Zirconium and UO_2," *J. Nucl. Mater.*, **509**, 517 (2018); https://doi.org/10.1016/j.jnucmat.2018.07.021.
17. A. CEZAIRLIYAN, J. L. MCCLURE, and A. P. MILLER, "Radiance Temperatures (in the Wavelength Range 523–907 nm) of Group IVB Transition Metals Titanium, Zirconium, and Hafnium at their Melting Points by a Pulse-Heating Technique," *Int. J. Thermophys.*, **15**, 993 (1994); https://doi.org/10.1007/BF01447109.
18. S. MASTROMARINO et al., "Assessment of Solid/Liquid Equilibria in the (U, Zr)O_{2+y} System," *J. Nucl. Mater.*, **494**, 368 (2017); https://doi.org/10.1016/j.jnucmat.2017.07.045.
19. T. G. THEOFANOUS et al., "In-Vessel Coolability and Retention of a Core Melt," *Nucl. Eng. Des.*, **169**, 1 (1997); https://doi.org/10.1016/S0029-5493(97)00009-5.
20. J. M. SEILER et al., "Consequences of Material Effects on In-Vessel Retention," *Nucl. Eng. Des.*, **237**, 1752 (2007); https://doi.org/10.1016/J.NUCENGDES.2007.03.007.
21. J. P. VAN DORSSELAERE et al., "The ASTEC Integral Code for Severe Accident Simulation," *Nucl. Technol.*, **165**, 293 (2009); https://doi.org/10.13182/NT09-A4102.